Journal of Energy and Power Engineering 19 (2025) 191-199
doi: 10.17265/1934-8975/2025.05.004

Theoretical Comparative Study of CSP and PV Power Generation Systems for Remote Areas

Awa Mar[1, 4], Serigne Thiao[2], Cheikh Mbow[3] and Issakha Youm[4]

1. Higher School of Engineering Sciences and Techniques, Amadou Makhtar MBOW University of Dakar (UAM), BP 45927 Dakar, Senegal

2. Laboratory of Chemistry and Physics of Materials (LCPM)/Department of Physics, Assane Seck University of Ziguinchor, BP 523 Ziguinchor, Senegal

3. Laboratory of Fluid Mechanical and Hydraulic, Department of Physics, Faculty of Sciences and Technology, University Cheikh Anta Diop of Dakar, BP 5005 Dakar, Senegal

4. Laboratory of Solar Energy, Materials and Systems, Department of Physics, Faculty of Sciences and Technology, University Cheikh anta Diop of Dakar, BP 5005 Dakar, Senegal

Abstract: This paper analyzes the sizing and modeling of a mini power plant using CSP (concentrated solar power) and PV (photovoltaic) technology, focusing on remote areas such as CERER in Senegal. The objective is to model a PT (parabolic trough) collector connected to an Ericsson engine following a Joule cycle in order to evaluate electricity production during a typical day in April. Two operating strategies are considered: "sun-dependent" and "fixed hours". The research includes modeling solar energy into usable heat using a PT Solar Courant collector, then into usable heat for work. The collector is characterized by high performance, low cost, and 80% optical efficiency with a collection area of 69.24 m². The results will enable a purely energy-based comparison, highlighting the efficiencies and collection areas between CSP and PV.

Key words: CSP (concentrated solar power), PV (photovoltaic), Ericsson engine, operating strategies, comparison.

Nomenclature

Latin Letters

Symbol	Designation	Unit
$c_{p,f}$	Specific mass heat capacity at constant pressure	$J.kg^{-1}K^{-1}$
D	Hydraulic diameter of the absorber tube	m
F	Shape factor	-
h_{conv}	Coefficient of forced convection of the heat fluid	$W.m^{-2}K^{-1}$
h_v	Coefficient of external mixed convection	$W.m^{-2}K^{-1}$
DNI	Direct Normal Insolation	$W.m^{-2}$
l_{conc}	Width of the concentrator	m
l_r	Perimeter of receiver tube	m
L_{conc}	Length of the concentrator	m
$\dot{m}$	Mass flow rate of the fluid	kgs^{-1}
P_m	Wetted perimeter of the absorber tube	m
$\dot{Q}_{conc}$	Thermal power emitted by the concentrator and received by the receiver	W
$\dot{Q}_{conv}$	Thermal power lost by convection	W
$\dot{Q}_f$	Thermal power received by the heat fluid	W
$\dot{Q}_r$	Thermal power transmitted from the receiver to the engine heat exchanger	W
$\dot{Q}_{ray}$	Thermal power lost by radiation	W
$\dot{Q}_s$	Thermal power emitted by the sun and received by the concentrator	W
Q_{sto}	Stored thermal energy	J
S	Fluid passage section	m^2
S_{conc}	Opening surface of the concentrator	m^2
S_m	Wetted surface of the receiver tube	m^2
S_r	Surface of receiving envelope	m^2
t	Time	S
T_0	Ambient temperature	K
T_{C-R}	Compressor outlet temperature, heat exchanger inlet temperature	K
T_{E-R}	Temperature at regulator outlet, temperature at heat exchanger inlet	K
T_f	Average temperature of the heat fluid in the tube	K
$T_f(x)$	Local temperature of the heat fluid	K
T_{fus}	Salt melting temperature	K

Corresponding author: Awa Mar, associate professor, research fields: solar thermal energy and energy conversion.

T_{in}	Input temperature of the heat fluid in the tube	K
T_{out}	Output temperature of the heat fluid in the tube	K
T_p	Average temperature of the wall of the receiver tube	K
$T_p(x)$	Local temperature of the wall of the receiver tube	K
T_{PT}	Temperature output PT expansion valve input	K
T_{PT-sto}	Storage outlet temperature regulator inlet temperature	K
$\dot{W}_{C,i}$	Indicated mechanical compression power	W
$\dot{W}_{C,real}$	Actual mechanical compression power	W
$\dot{W}_{E,i}$	Indicated mechanical expansion power	W
$\dot{W}_{E,real}$	Actual mechanical expansion power	W
$\dot{W}_{elec}$	Electrical power generated by the alternator	W
$\dot{W}_{i,net}$	Indicated net mechanical power	W
$\dot{W}_{net}$	Net mechanical power	W

Greek Characters

α_{conc}	Geometric concentration ratio $\alpha_{conc} = \frac{S_{conc}}{S_r}$	-
α_r	Absorption coefficient of the receiver tube	-
β	Pressure ratio	-
ε	Emissivity coefficient of the receiver tube	-
ε_R	Recovery efficiency	-
ζ_{conc}	Geometrical efficiency of the concentrator	-
κ_{PT}	Effective efficiency of the PT	-
λ	Thermal conductivity of the fluid	$W.m^{-1}K^{-1}$
μ	Dynamic viscosity of the fluid	Pa. s
η_{conc}	Optical efficiency of the concentrator	-
η_{elec}	Alternator efficiency	-
η_{engine}	Engine efficiency	-
$\eta_{meca,C}$	Mechanical compression efficiency	-
$\eta_{meca,E}$	Mechanical expansion efficiency	-
η_{S-elec}	Solar to electricity conversion efficiency	-
η_{th-PT}	Thermal global efficiency of the PT	-
ρ_{conc}	Optical efficiency of reflection	-
σ_{SB}	Stefan Boltzmann constant	$W.m^{-2}K^{-4}$
τ_{conc}	Optical efficiency of transmission	-

1. Introduction

The issue of sizing solar thermal power plants has been addressed in several different ways without the aim of establishing a general method [1-3].

As a high-performance clean energy source, hybrid CSP (concentrated solar power)-PV (photovoltaic) power generation delivers reliable, clean, and continuous energy across multiple scenarios, including electricity, heating, hydrogen and oxygen production, making it ideal for high-altitude regions [4]. Hybrid concentrated solar power (CSP) and PV (photovoltaic) systems, known for clean energy attributes and robust grid-support capabilities, have emerged as a viable and cost-effective solution. The hybridization of solar PV and CSP systems has many benefits. Hybrid PV-CSP systems enable the simultaneous generation of electricity and heat, maximizing the use of solar energy, particularly in sun-rich areas like Cameroon [5]. Yu et al. [6] propose a novel Carnot Battery system based on an open-cycle ultra-high-temperature heat pump and a tower CSP (concentrated solar power) configuration. In their study, thermodynamic models for charging/discharging cycles and solar plants were established for a system with 10 MW power output and the results show that the proposed system achieves a round-trip efficiency of 56.2% under typical operating conditions, with a potential increase to 62.5% at lower discharging pressure ratio. Concentrated solar power generation is a promising technology that relies on the concentration of solar radiation to drive a heat engine and generate electricity. Fang et al. [7] are carried out an OIES (off-grid integrated energy system) combining PV (photovoltaic), CSP (concentrated solar power), TES (thermal energy storage), and EES (electrochemical energy storage) is designed to minimize both the LCoE (levelized cost of energy) and LPSP (loss of power supply probability). Scenario comparisons show that a CSP + TES configuration alone cuts LCOE by 14.17% and LPSP by 3.24%, yet causes PV curtailment. Compared to solar PV and onshore wind alternatives, CSP cannot currently compete on the levelized cost of electricity (LCoE) [8]. Also accord to Adak et al. [9], the levelized cost of energy (LCoE) of solar energy driven power systems is expected to drop ~ 3 ¢/kWh for utility scale solar PV and 5 ¢/kWh for baseload CSP power plants by 2030. An evaluation of two solar technologies—PV (photovoltaic) and PT-CSP (parabolic trough) CSP technology was conducted by Okeke et al. [10] under specific geographical and techno-economic criteria to support solar electricity and green hydrogen development across Nigeria. Their results indicate that 105.63 GWe of grid capacity is required to meet Nigeria's energy demand, whereas 57.32 GWe from grid-connected solar plants needed to replace unsustainable grid supplying 54.3% of estimated population. Almetwally et al. [11] examine the current state of solar-powered RO (reverse osmosis) desalination, focusing on technological advancements, integration strategies, and prevailing challenges. The analysis encompasses various configurations, including PV (photovoltaic) systems, CSP (concentrated solar power), and hybrid models, assessing their performance, efficiency, and applicability across different geographical contexts. CSP offers greater dispatchability and reliability by integrating TES (thermal energy storage), which allows excess thermal energy collected during the day and used at night or during peak demand [12]. CSP (concentrated solar power) equipped with integrated thermal storage offers a groundbreaking solution. It delivers dispatchable electricity and functions as a large, cost-effective thermal "battery", making it an ideal complement to wind and PV by storing solar heat for use during nighttime or cloudy conditions [13].

We will size a mini-CSP (concentrated solar power) plant of a few dozen kWh for the CERER site in Senegal. To do this, we will model a parabolic trough collector coupled with an Ericsson open Joule cycle engine with recovery adapted to electricity production. The aim is to evaluate the electrical energy produced by a given installation of components on a typical day in April, which is the sunniest month. We will assume two operating strategies: "sun-dependent" and "fixed hours". Next, we will compare the energy and collection areas of CSP and PV (photovoltaic) solar energy.

2. Materials and Method

2.1. Modeling Solar Energy into Usable Heat

We will model a PT (parabolic trough) collector consisting of a cylindrical-parabolic concentrator and a linear receiver. This sensor will be referred to as the PT Solar Courant collector. To find the outlet temperature of the heat transfer fluid, which will be the working fluid temperature of the engine, we start with the energy balance equation for an elementary volume at the absorber tube (Fig. 1) [14, 15].

The PT collector operates according to the following system:

$$\begin{cases} \kappa_{PT} DNI.\, l_{conc} = h_{conv} P_m \left(T_p(x) - T_f(x)\right) \\ \qquad + h_v l_r \left(T_p(x) - T_0\right) \\ \qquad + \epsilon\sigma F l_r \left(T_p(x)^4 - {T_0}^4\right) \\ \dot{m} c_{p,f} \dfrac{dT_f}{dx} = h_{conv} P_m \left(T_p(x) - T_f(x)\right) \end{cases} \tag{1}$$

$$\dot{Q}_s = DNI\, S_{conc} \tag{2}$$

$$\dot{Q}_{conc} = \alpha_r \eta_{conc}\, DNI.\, S_{conc} \tag{3}$$

$$\dot{Q}_r = \dot{Q}_{conc} - h_v\, S_r\, (T_r - T_0) - \sigma_{SB}\, F\varepsilon S_r (T_r^4 - T_0^4) \tag{4}$$

$$\eta_{th-PT} = \frac{\dot{Q}_r}{\dot{Q}_s} \tag{5}$$

We assume a collector that offers high performance at low cost, with proven reliability and longevity. It has high optical precision with an optical efficiency η_{conc} of 80% and a high level of solar tracking. The length of a module L_{conc} is 12 m by $l_{conc} = 5.77$ m wide, giving a collection area of $S_{conc} = 69.24$ m^2. It is easy for a glassmaker to reproduce. It is rigid in torsion and bending, corrosion-resistant, and can withstand winds of up to 31.5 ms^{-1} [16].

We will model a receiver tube with an outer diameter of 23 mm, giving an outer perimeter of $l_r = 72$ mm. It has an absorbance $\alpha_r \geq 0.95$ (rounded to 1) and an emissivity $\varepsilon \leq 0.14$.

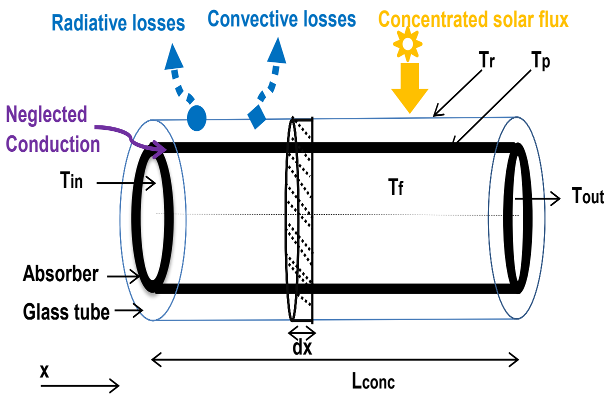

Fig. 1 Schematic diagram of the collector.

Table 1 PT Solar Courant collector specifications used for sizing.

Parameters	Values
L_{conc}	12 m
l_{conc}	5.77 m
α_{conc}	80
l_r	$7.2.10^{-2}$ m
P_m	$4.7.10^{-2}$ m
η_{conc}	0.8
α_r	1
$\varepsilon.F$	0.10

Thus, the geometric concentration ratio of the sensor used for sizing will be 80. Its characteristics are summarized in Table 1.

2.2 Modeling Heat in Indicated Work

Using an approach similar to that of other authors [17], we consider an Ericsson engine operating according to Joule's thermodynamic cycle in an open cycle. It is a reciprocating engine with external heat input, separate compression and expansion chambers, recovery, and a single-phase gaseous working fluid. The working fluid is air, which is treated as an ideal gas with constant specific heat. The air is recycled, without renewal as in any external combustion engine, which therefore requires two heat sources. The cold source is atmospheric air and the hot source is provided in the form of heat from the parabolic trough concentrator.

The system describes a cycle of elementary transformations that we will assume to be reversible in order to study them more easily. The Joule cycle consists of two isentropic and two isobaric processes.

The successive stages of the thermodynamic cycle are represented in a Temperature Entropy diagram (Fig. 2). The air cycle consists of an isentropic compression (P_{max}) of atmospheric air at T_0 inside the compression cylinder C (0 → C-R), an isobaric preheating of the air by the recuperator R (C-R → R-PT), an isobaric heating of the air by the parabolic trough concentrator PT (R-PT → PT), an isentropic expansion in the expansion cylinder E (PT → E-R), the isobaric transfer of heat to the recuperator R (E-R → R-0), and finally a return to atmospheric temperature T_0, at atmospheric pressure P_0.

We assume that the thermal power transmitted by the receiver $\dot{Q}_r$ to the engine's heat exchanger is received in its entirety by the engine's working fluid. The recuperator R is considered to be a perfect heat exchanger, with no thermal losses. Pressure losses are not taken into account, and only the PT is diabatic.

2.2.1 Determination of Cycle Power and Efficiency

The equations governing the system are described below, and the engine characteristics are given in Table 2.

$$\dot{W}_{i,net} = \dot{W}_{E,i} - \dot{W}_{C,i} \quad (6)$$

$$\dot{W}_{E,i} = \dot{m}c_{p,air}(T_{PT} - T_{E-R}) \quad (7)$$

$$\dot{W}_{C,i} = \dot{m}c_{p,air}(T_{C-R} - T_0) \quad (8)$$

$$\dot{W}_{net} = \dot{W}_{E,real} - \dot{W}_{C,real} \quad (9)$$

$$\dot{W}_{C,real} = \dot{W}_{C,i}/\eta_{meca,C} \quad (10)$$

$$\dot{W}_{E,real} = \eta_{meca,E} \times \dot{W}_{E,i} \quad (11)$$

$$\eta_{engine} = \dot{W}_{net}/\dot{Q}_r \quad (12)$$

By introducing an alternator with efficiency η_{elec} mechanical energy $\dot{W}_{net}$ will be converted into electrical energy with power $\dot{W}_{elec}$:

$$\dot{W}_{elec} = \eta_{elec} \times \dot{W}_{net} \quad (13)$$

$$\eta_{S-elec} = \dot{W}_{elec}/\dot{Q}_s \quad (14)$$

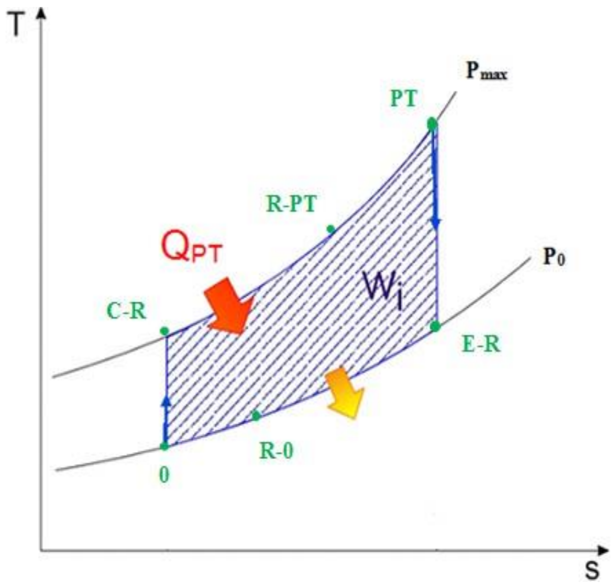

Fig. 2 (T, S) diagram of the Joule cycle with heat recovery.

Table 2 Ericsson engine specifications used for sizing.

Parameters	Values
$\eta_{meca,C}$	0.9
$\eta_{meca,E}$	0.9
ε_R	0.8

3. Results and Discussions

3.1 Production "Sun-Dependent"

For solar power generation, the load curve is not fixed; you choose when to generate electricity and at what load. It should be noted that in hot regions, peaks in electricity demand often coincide with peaks in sunlight. In this case, the design of a solar installation requires knowledge of: the nature of the installation and the solar irradiation at the installation site [14, 15]. The thermodynamic cycle will be variable and the high temperature of the cycle will continue to change throughout the day depending on the irradiation.

We will first look at the evolution of the TPT collector outlet temperature over time (Fig. 3).

The temperatures obtained are generally satisfactory, reaching over 1,200 K.

Using the same principle, the instantaneous electricity production and the efficiencies of the collector η_{th-PT} and the engine η_{engine} (Fig. 4) evolve with the selected flow rate and pressure ratio.

Like the temperature of the fluid at the collector outlet, the electrical power $\dot{W}_{elec}$ varies with time and therefore with the DNI, which is the key factor in concentration systems. With this sensor, we also note that its thermal efficiency varies between $\sim$ 57% and $\sim$ 72%. It should be remembered that the ideal energy efficiency that this collector could achieve is $\eta_{th-PT} = \eta_{conc} = 80\%$, with the absorption coefficient of the receiver tube being $\alpha_r = 1$. However, we can see that the engine efficiency η_{engine} varies little over time, and is generally between 10% and less than 14%. This collector is quite powerful and could be used with other more powerful thermodynamic cycles.

With this study, we were also able to calculate the average efficiencies of the collector η_{th-PT} = 70% and the engine η_{engine} = 13%.

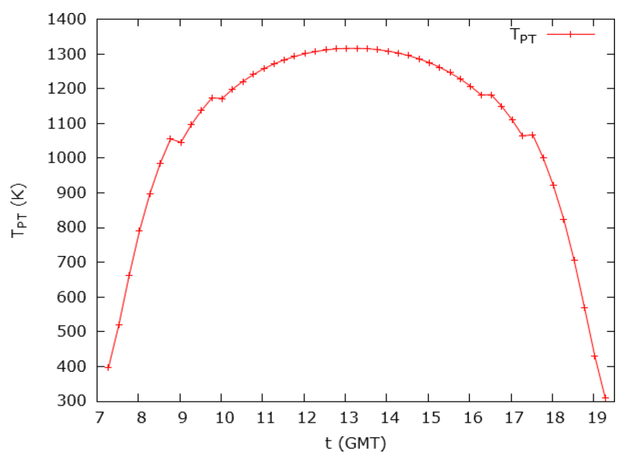

Fig. 3 Change in the output temperature of the T_{PT} collector over time.

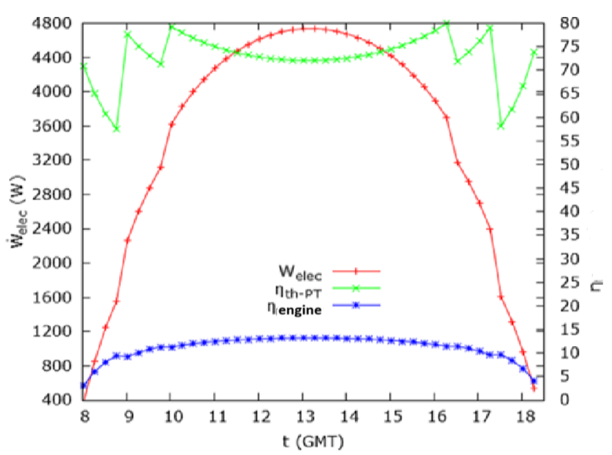

Fig. 4 Instantaneous optimal electricity production and evolution of the efficiencies.

3.2 Production at "Fixed Hours"

For production at set times, the charging or discharging curves will be fixed. The site's energy requirements must be known. The integration of thermal storage will provide a permanent source of heat. The high temperature of the cycle will be constant and equal to the outlet temperature of the storage T_{PT-sto}. With this collector, we will size up the thermal storage load to deduce the overall daily production. We will use Table 3 to obtain the daily irradiation.

Regardless of the engine, we are primarily interested in the amount of heat stored. The storage is such that during production, we will always have a mixture of solid and liquid to remain in a phase change state and have the T_{PT-sto} temperature equal to the melting temperature of the salt $T_{fus} = 716$ K. It is important to remember its latent heat of fusion L_f, which is -241,000 J.kg^{-1}.

On a typical day in April, the daily DNI is 6,690 W.h.m^{-2}.day^{-1}. The surface area of the concentrator $S_{conc} = 69.24$ m^2 receives thermal energy Q_S = 463,215.6 W.h.day^{-1} from the sun per day. With an optimal thermal efficiency η_{th-PT} of 70% for the collector and assuming that there are no heat losses between the receiver and the storage system, the amount of heat stored with the collector would be 324,250.9 W.h.day^{-1}. This thermal energy Q_{sto} will enable the salt to be brought from the ambient temperature T_0 to the melting temperature T_{fus} (in the form of sensible heat) and to remain there (in the form of latent heat).

$$Q_{sto} = m_{salt}c_{p,salt}(T_{fus} - T_0) + m_{salt}L_f \qquad (15)$$

with: m_{salt} is the mass of the storage salt to be determined and $c_{p,salt}$ is its heat capacity.

The heat capacities of salts are often determined experimentally, or estimated and weighted based on the molar fraction of their components. In general, the thermal capacity of molten salts varies little with temperature. The specific heat capacity $c_{p,salt}$ of the eutectic mixture of sodium chloride and magnesium chloride salts ($NaCl/MgCl_2$) at 42% mol $MgCl_2$ is 1,087 Jkg^{-1}K^{-1}.

To store a quantity of heat Q_{sto} of 324,250.9 W.h.day^{-1}, a minimum mass of salt m_{salt} of 1,684 kg is required, i.e., a volume of approximately ~ 1 m^3 with the density of liquid $NaCl/MgCl_2$, which is 1,680 kg.m^{-3}. It should be noted that these salts are very inexpensive.

With the aim of always having a mixture of solid and liquid in storage, only part of the latent heat will be used to generate electricity (i.e., a maximum of 112,731 Wh). We will consider an engine with an efficiency of 12% (with a high cycle temperature of T_{fus} = 716 K; the engine's performance will be revised downwards) coupled with an alternator with an electrical efficiency of 90%. The maximum total electrical energy W_{elec} that could be produced during a typical day in April would then be 12,175 W.h. The solar-to-electric conversion efficiency would then be η_{S-elec} = 2.63%. We note that this efficiency is low; without storage, the efficiency was 7.7%. In fact, there is a penalty incurred by storage because, as we have seen Fig. 2, the outlet temperature of the fluid from the collector often exceeds T_{fus} = 716 K. However, if we had used the heat produced by the collector directly, we would have had a higher cycle temperature than T_{fus} and therefore more electricity (Fig. 5). The high temperature of the cycle is a direct factor in electrical power. However, the advantage of storage remains the ability to anticipate production, given that solar resources are highly unpredictable. To offset the penalties incurred by storage, we can consider a control loop that allows for simultaneous storage and production, using storage as a last resort.

Under the same operating conditions, we extrapolate to determine the daily production for all other months of the year (Table 3).

With production at fixed times via storage, the energy produced is generally slightly above 10 kWh, except in July, August, and September (the rainy season). This constraint can be circumvented by integrating hybridization with another energy source.

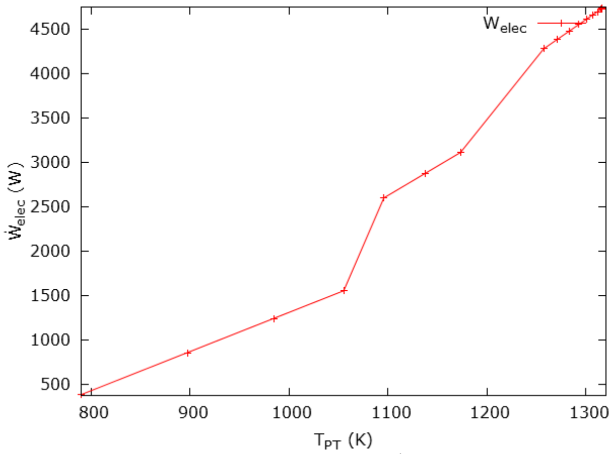

Fig. 5 Evolution of electrical power $\dot{W}_{elec}$ as a function of temperature T_{PT}.

Table 3 Daily electricity production.

Month	$\dot{Q}_s$ (kWh/day)	W_{elec} (kWh/day)
January	404.4	10.63
February	436.9	11.48
March	481.9	12.66
April	463.2	12.18
May	490.2	12.88
Jun	446.6	11.74
July	366.9	9.64
August	326.1	8.57
September	331.6	8.72
October	415.4	10.92
November	427.2	11.23
December	412.7	10.85
Average	416.8	10.95

3.3 Comparison with Photovoltaic Systems

Due to its modularity and ease of operation, photovoltaics are gaining ground over CSP for small to medium-sized installations.

Less popular and less mature than photovoltaic solar energy, CSP is nevertheless more advantageous, especially for medium and large installations. However, above a certain power level, photovoltaic and CSP will be in direct competition [18, 19]. But where should we draw the line between medium and high power? To confirm the advantage of CSP over PV for medium power, we will conduct a comparative study of our thermodynamic system and the MACSEN-PV project's pilot PV plant located at the CERER center.

This pilot facility is intended to serve as:

- A technology demonstration platform for this type of facility;
- A test bed for the various operating conditions that may be encountered in the Senegalese electricity grid;
- A teaching aid for the training of local technicians.

With a power output of 3.15 kW_P it consists of 18 polycrystalline silicon cell modules covering a total area of 23.4 m^2. It has a room equipped with two inverters. The first (3.2 kW) is a grid-connected inverter that generates alternating current from the photovoltaic modules. The second (2.2 kW) generates current from the batteries and starts up in the event of a grid failure. It is also used to charge the battery bank (capacity (C10) per unit: 816 Ah). The room is also equipped with measurement and control systems.

The purpose of our theoretical comparison between CSP and solar PV is purely energetic and not economic. To do this, we will reduce the surface area of the PV modules to the same surface area as the solar field of the collector, i.e., 69.24 m^2. Thus, with a 90% efficiency injection inverter and 80% module efficiency, the electrical power delivered by a surface area of 69.24 m^2 would be: $\dot{W}_{elec}$ = 6.7 kW, i.e., a solar-to-electric conversion efficiency of 9.7%.

To determine the electrical power of our CSP system for comparison purposes, we will use the same STC (standard test conditions) as for PV, i.e., AM1.5 spectrum under 1,000 W/m^2 irradiance and an ambient temperature of 25 °C or 298 K. With more consistent sunlight, we used a pressure ratio of $\beta = 7$ and an air flow rate of $\dot{m}$ = 0.02 kgs^{-1}. The electrical power delivered would then be $\dot{W}_{elec}$ = 12.3 kW with a thermal efficiency of the collector η_{th-PT} = 76.9% and a solar-to-electric conversion efficiency of η_{s-elec} = 25.6%. This result is unequivocal and proves that CSP is more promising than photovoltaics. It has been proven that PV requires much more space and has a lower conversion efficiency: in the case of PV, commercial cells have an efficiency of 12% to 15%, while CSP has an efficiency of around 20% [18, 19].

Currently, CPV (concentrated photovoltaics), a niche technology, is revolutionizing the solar energy market. According to the German Fraunhofer ISE (Institute for Solar Energy) Systems and the American NREL (National Renewable Energy Laboratory), the price of CPV modules is expected to fall by 2030 to a level competitive with conventional modules. Recently, the market has been moving towards Micro-CPV (miniaturization of components to reduce costs) and hybrid systems combining photovoltaic and thermal energy [20]. Regardless of the technology used, the main input factor remains sunlight, and it offers a reliable solution for energy generation in the sunny regions where we live.

4. Conclusion

In this study, we designed a mini power plant with a capacity of around 10 kW using two different approaches. Regardless of the method used, solar energy remains highly unpredictable, and the hourly distribution of sunlight is the key factor in electricity production. The most influential factors are also electricity demand and installed capacity. However, we cannot comment on the price of solar thermal electricity due to the lack of a market. This study also allowed us to confirm that storage, although beneficial for smoothing and forecasting production, remains a penalty from an energy perspective. In general, a basic solar field module must be sized, and for the rest, the number of modules required per row must be added. The comparison between solar PV and solar CSP allowed us to see the advantages of the latter, particularly in terms of space savings and efficiency.

Although the results obtained depend on the performance of certain parameters relating to the characteristics of the collector and engine, they are acceptable and realistic. The technologies modeled and dimensioned are feasible. These results now need to be validated experimentally.

References

[1] Beltagy, H., Semmar, D., Mihoub, S., and Said, N. August 2016. "Sizing Analysis of Linear Fresnel Solar Thermal Power Plant in Algeria." *Energy Procedia* 93: 19-24. https://doi.org/10.1016/j.egypro.2016.07.144.

[2] Xu, B., Li, P. W., Chan, C., and Tumilowicz, E. 15 February 2015. "General Volume Sizing Strategy for Thermal Storage System Using Phase Change Material for Concentrated Solar Thermal Power Plant." *Applied Energy* 140: 256-68. https://doi.org/10.1016/j.apenergy.2014.11.046.

[3] Chen, R., Rao, Z. H., and Liao, S. M. 1 December 2018. "Determination of Key Parameters for Sizing the Heliostat Field and Thermal Energy Storage in Solar Tower Power Plants." *Energy Conversion and Management* 177: 385-94. https://doi.org/10.1016/j.enconman.2018.09.065.

[4] Wang, Y., Guan, Z. W., Yao, L. X., Luo, S. Y., Zhang, B. Q., and Xiao, X. Y. November 2025. "Energy Transition in High-Altitude Regions: The Role of Hybrid CSP-PV Plants." *Sustainable Energy Technologies and Assessments* 83: 104591. https://doi.org/10.1016/j.seta.2025.104591.

[5] Flora, F. M. I. 6 March 2025. "An MCDM-GIS Based Site Suitability Analysis for Solar Power Plant Integration in Cameroon: Solar Hybridization to Optimize Green Electricity and Hydrogen Production (2025)." *International Journal of Hydrogen Energy* 106: 23-51. https://doi.org/10.1016/j.ijhydene.2025.01.445.

[6] Yu, J., Jia, T., Gao, Z. Z., Gu, X. Z., Tan, C. Z., Zhao, Y., and Dai, Y. J. 30 October 2025. "Carnot Battery with Open-Cycle Ultra-High-Temperature Heat Pump for Large-Scale Hybrid PV and Concentrating Solar Power Plants (2025)." *Energy* 335: 138385. https://doi.org/10.1016/j.energy.2025.138385.

[7] Fang, R. M., and Deng, X. C. January 2026. "Optimization Configuration of Integrated Energy System in Plateau Mining Areas Considering the Coordination of Economy and Reliability (2026)." *Sustainable Energy Technologies and Assessments* 85: 104761. https://doi.org/10.1016/j.seta.2025.104761.

[8] Khan, M. I., Gutiérrez-Alvarez, R., Asfand, F., Bicer, Y., Sgouridis, S., Al-Ghamdi, S. G., Jouhara, H., Asif, M., Kurniawan, T. A., Abid, M., Pesyridis, A., and Farooq, M. August 2024. "The Economics of Concentrating Solar Power (CSP): Assessing Cost Competitiveness and Deployment Potential (2024)." *Renewable and Sustainable Energy Reviews* 200: 114551. https://doi.org/10.1016/j.rser.2024.114551.

[9] Adak, D., Bhattacharyya, R., and Barshilia, H. C. May 2022. "A State-of-the-Art Review on the Multifunctional Self-Cleaning Nanostructured Coatings for PV Panels, CSP Mirrors and Related Solar Devices (2022)." *Renewable and Sustainable Energy Reviews* 159: 112145. https://doi.org/10.1016/j.rser.2022.112145.

[10] Okeke, C. J., Egberibine, P. K., Edet, J. U., Wilson, J., and Blanchard, R. E. June 2025. "Comparative Assessment of Concentrated Solar Power and Photovoltaic for Power Generation and Green Hydrogen Potential in West Africa: A Case Study on Nigeria (2025)." *Renewable and Sustainable Energy Reviews* 215: 115548. https://doi.org/10.1016/j.rser.2025.115548.

[11] Almetwally, E. M., Elazab, M. A., Kabeel, A. E., Yasser, Y., and Elgebaly, A. 15 November 2025. "Solar Powered Reverse Osmosis Desalination: A Systematic Review of Technologies, Integration Strategies and Challenges (2025)." *Desalination* 615: 119228. https://doi.org/10.1016/j.desal.2025.119228.

[12] Dai, X. Y., Fang, Y. J., Gedik, E., Li, Z., and Wirsum, M. 15 February 2026. "PV-CSP Hybrid System Configuration and Performance Based on Simulation and Mathematical Methods (2026)." *Renewable Energy* 258: 125020. https://doi.org/10.1016/j.renene.2025.125020.

[13] Zhou, H. R., Guo, A. X., Wang, D. L., Yang, Y., Yang, S. Y., and Mo, W. L. February 2026. "Multi-scale Complementarity and Integrated Optimization Analysis of a Wind-PV-CSP Hybrid System for Off-Grid Hydrogen Production (2026)." *Journal of Environmental Chemical Engineering* 14 (1): 120762. https://doi.org/10.1016/j.jece.2025.120762.

[14] Mar, A., Mbow, C., Thiao, S., and Youm, I. 2014. "Theoretical Study of a Parabolic Trough Solar Collector: Influences of Atmospheric Parameters." *International Journal of Energy, Environment, and Economics* 22 (5): 461-73.

[15] Mar, A., Thiao, S., Mbow, C., and Youm, I. 2016. "Study of a Parabolic Trough Adequate for the CERER Site (Dakar-Senegal)." *Journal of Energy and Power Engineering* 10 (5): 275-82.

[16] Kearney, D. W. 2007. "Parabolic Trough Collector Overview: Notes on a Bit of History, Development after Luz, and a Recent Surge in Trough Collector Technology Offerings." Parabolic Trough Workshop 2007 at the National Renewable Energy Laboratory, Golden CO, USA.

[17] Bonnet, S., Alaphilippe, M., and Stouffs, P. December 2005. "Energy, Exergy and Cost Analysis of a Micro-cogeneration System Based on an Ericsson Engine." *International Journal of Thermal Sciences* 44 (12): 1161-8. https://doi.org/10.1016/j.ijthermalsci.2005.09.005.

[18] Chiang, A. C., Moore, M. R., Johnson, J. X., and Keoleian, G. A. October 2016. "Emissions Reduction Benefits of Siting an Offshore Wind Farm: A Temporal and Spatial Analysis of Lake Michigan." *Ecological Economics* 130: 263-76. https://doi.org/10.1016/j.ecolecon.2016.07.010.

[19] Ghirardi, E., Brumana, G., Franchini, G., and Perdichizzi, A. December 2021. "The Optimal Share of PV and CSP for Highly Renewable Power Systems in the GCC Region." *Renewable Energy* 179: 1990-2003. https://doi.org/10.1016/j.renene.2021.08.005.

[20] Allouhi, A., Rehman, S., Buker, M. S., and Said, Z. March 2023. "Recent Technical Approaches for Improving Energy Efficiency and Sustainability of PV and PV-T Systems: A Comprehensive Review." *Sustainable Energy Technologies and Assessments* 56: 103026. https://doi.org/10.1016/j.seta.2023.103026.